Proceedings of the ASME 2010 3rd Joint US-European Fluids Engineering Summer Meeting and 8th International Conference on Nanochannels, Microchannels, and Minichannels
FEDSM-ICNMM2010
August 1-5, 2010, Montreal, Canada

FEDSM-ICNMM2010-30752

A NON-LOCAL CONVECTIVE FLUX LIMITER FOR UPWIND-BIASED FINITE VOLUME SIMULATIONS

Nicole M. W. Poe and D. Keith Walters
CAVS SimCenter
Department of Mechanical Engineering
Mississippi State University
Mississippi State, Mississippi, 39762

ABSTRACT

Finite volume methods on structured and unstructured meshes often utilize second-order, upwind-biased linear reconstruction schemes to approximate the convective terms, in an attempt to improve accuracy over first-order methods. Limiters are employed to reduce the inherent variable over- and under-shoot of these schemes; however, they also can significantly increase the numerical dissipation of a solution. This paper presents a novel non-local, non-monotonic (NLNM) limiter developed by enforcing cell minima and maxima on dependent variable values projected to cell faces. The minimum and maximum values for a cell are determined primarily through the recursive reference to the minimum and maximum values of its upwind neighbors. The new limiter is implemented using the User Defined Function capability available in the commercial CFD solver Ansys FLUENT. Various simple test cases are presented which exhibit the NLNM limiter's ability to eliminate non-physical oscillations while maintaining relatively low dissipation of the solution. Results from the new limiter are compared with those from other limited and unlimited second-order upwind (SOU) and first-order upwind (FOU) schemes. For the cases examined in the study, the NLNM limiter was found to improve accuracy without significantly increasing solution convergence rate.

INTRODUCTION

Crucial to many computational fluid dynamics (CFD) simulations is the discretized advection-diffusion equation, which manifests itself in all equations of transport. Simple solution techniques use first-order discretization schemes for the convective (advective) term; however, computed solutions experience severe and often unacceptable levels of numerical dissipation. Therefore, higher-order schemes have been developed to improve solution accuracy. For simulations on unstructured meshes, second-order schemes are most common. Application of these schemes for calculation of the convective term is successful in decreasing the numerical dissipation; although, higher-order methods also result in oscillations in regions of discontinuity or steep local gradient, as expressed by Godunov's Theorem [1]. The concept of a limiter that will eliminate oscillations by restoring monotonicity at discontinuities has been examined by numerous authors, but the success of this approach has yielded mixed results. For most existing flux limiting schemes, oscillations are reduced at the expense of re-introduction of a portion of dissipation [2].

Various limiters for use with higher-order schemes have been proposed in the literature. Early, smooth limiters proposed by Van Leer in 1974 [3] and Van Albada et al. in 1982[4] are capable of virtually eliminating oscillations; however, both force a smoothing of the solution at discontinuities. In 1981, Roe and Baines designed the Superbee limiter [5], reducing the smoothing behavior of existing limiters at the expense of slightly compressing the gradients in the solution. In 1988, Gaskell and Lau exhibited the higher-order SMART limiter [6], which possesses local third order accuracy [2]. The so-called Barth limiter was proposed in 1989 [7], providing a limiter specifically designed for use with unstructured grids. In 1993, Venkatakrishnan expanded upon the Barth limiter [8]. The novel limiter that resulted consists of a polynomial function, which is continuously differentiable; the Venkatakrishnan limiter also is not applied in regions of the domain where nearly uniform flow exist, allowing for computational savings. Michalak and Olliver-Gooch developed another similar limiter in 2008 [9], comprised of a different polynomial function and performing better than the limiter of Venkatakrishnan. While each new limiter continued to improve upon its predecessors potential areas of improvement remain. These include smoothing of

discontinuities and damping of naturally occurring extrema in smooth regions of the variable field.

Recent progress in the area of limiter improvement has focused in several different areas, one being in the detailed examination of the convective boundedness criterion (CBC) originally proposed by Gaskell and Lau [6]. Long considered a necessary and sufficient condition for bounded, normalized convective schemes, Yu et al. [10] proved the condition merely sufficient in their introduction of the extended convective boundedness criterion (ECBC). Further investigation demonstrated both the ECBC and CBC to be limiting cases of a general convective boundedness criterion (GCBC) [11]. In these studies, limiters were developed to constrain the normalized convective gradient within the bounds of the various proposed criteria. The limiters were able to virtually eliminate oscillations in the solution; however, a significant amount of numerical dissipation remained present in the results.

Monotonic limiters for use with higher-order total variation diminishing (TVD) schemes have also been thoroughly investigated. The combination of the Minmod limiter and ELED (Essentially Local Extremum Diminishing) scheme limiter [12] shows improvement over other TVD limiters; although, some numerical dissipation still exists. Limiters for compact TVD (CTVD) schemes [13] and characteristic variable-based limiters [14] have been developed with similar results. These advances demonstrate the necessity of a superior limiter in order to obtain an optimum higher-order scheme.

Most flux limiting schemes to date, including the CBC and TVD based schemes mentioned above, are formulated with local data, i.e. the flux variables are computed entirely from cell data in the neighbor stencil. While computationally attractive, this approach may restrict the capability of the limiters. The primary difficulties encountered thus far lie in the fact that limiters which enforce monotonicity near discontinuities also tend to limit or "clip" naturally occurring extrema in smooth regions of the variable field, manifesting as extra dissipation in the solution. Ideally, a flux limiting scheme will eliminate non-physical oscillations near steep gradients while reproducing smooth regions in a manner identical to an unlimited second-order scheme.

This paper presents a new contribution to limiter development for use with upwind-biased, finite-volume CFD algorithms on structured and unstructured grids. Instead of formulating the limiter function solely on neighbor (local) cell data, the dependent variable extrema within any given cell are estimated by recursive examination of extrema in upwind neighbor cells. Reconstructed face values are then constrained to satisfy boundedness within these estimates. The goal of this paper is to present the derivation of a non-monotonic (NLNM) limiter of this type and to demonstrate its improved performance over existing limited and unlimited second-order and first-order methods for simple test cases.

The remainder of the paper is organized as follows. The next section presents the numerical method, including details on the development of the new limiter, and contrasts it with existing limiter methods for second-order upwind schemes. Next, the new limiter is applied to several simple test cases to demonstrate its ability to reduce oscillations while maintaining low numerical dissipation on Cartesian and unstructured triangular meshes; the computational cost of the recursive limiter is also examined. The final section provides conclusions and outlines future work.

NOMENCLATURE

Φ	scalar variable
t	time
x,y	spacial coordinates
ρ	density
$\boldsymbol{v}$	velocity vector
Γ	diffusivity coefficient
S	source term
A	area
$\dot{m}$	mass flow rate
$\boldsymbol{r}$	position vector
$\hat{n}$	unit outward normal vector
V	cell volume
α	limiter
D	dissipation

Subscripts

Φ	of the scalar variable, Φ
j	vector index notation
f	face centroid
n	cell node
U	centroid of upwind neighbor cell
D	centroid of downwind neighbor cell
C	centroid of current cell
MAX	maximum value
MIN	minimum value
nbr	upstream neighbor cell
in	entering a cell
out	exiting a cell

Superscripts

*	value at cell node
′	value at upstream neighbor cell
″	value at cell based on upwind neighbors

NUMERICAL METHOD

Background

The specific class of numerical methods addressed in this paper is the finite-volume approach with upwind-based reconstruction of the convective terms. As a representative problem, we consider the general scalar advection-diffusion equation. All results in this paper were obtained from the commercially available CFD solver, FLUENT version 6.2.16, from ANSYS, Inc. [15]. The new limiter presented in this work was implemented using the User Defined Function capability available with that code. Simulations were performed using the steady state, implicit solver.

For an arbitrary scalar quantity Φ, the general governing transport equation is

$$\frac{\partial}{\partial t}\left(\rho\Phi\right)+\frac{\partial}{\partial x_j}\left(\rho v_j\Phi\right)=\frac{\partial}{\partial x_j}\left(\Gamma\frac{\partial\Phi}{\partial x_j}\right)+S_\Phi \qquad (1)$$

Here ρ is the fluid density, $\boldsymbol{v}$ is the fluid velocity, Γ is the diffusivity coefficient, and S_Φ is an arbitrary source term. For the steady case with no sources or sinks, the transport equation integrated over a finite control volume (cell) becomes:

$$\int_{CS} \rho v_j \Phi dA = \int_{CS} \Gamma \frac{\partial \Phi}{\partial x_j} dA \qquad (2)$$

where the subscript CS denotes integration over the bounding surface of the cell. Discretizing this reduced finite volume equation transforms the surface integral into a summation over the faces of the cell.

$$\sum_{f=1}^{\#\,faces} \rho_f \Phi_f \left(\hat{n}_j v_j\right) A_f = \sum_{f=1}^{\#\,faces} \Gamma \left(\hat{n}_j \frac{\partial \Phi}{\partial x_j}\right) A_f \qquad (3)$$

Here ***v*** is the average face velocity, ***n*** is the outward-pointing unit normal vector, Φ_f is the average face value of the dependent variable, and A_f is the face area. The equation may be expressed more simply in terms of face mass flow rates as:

$$\sum_{f=1}^{\#\,faces} \dot{m}_f \Phi_f = \sum_{f=1}^{\#\,faces} \Gamma \left(\hat{n}_j \frac{\partial \Phi}{\partial x_j}\right) A_f \ . \qquad (4)$$

In general, discrete values for Φ are stored at each cell centroid; however, the values of Φ_f used in the numerical representation of the convective term must be determined via reconstruction from this known centroid data.

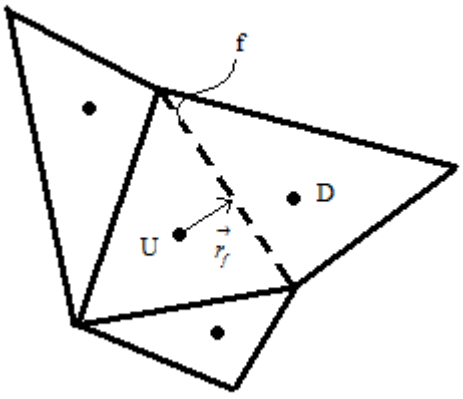

Figure 1. Unstructured grid. For the examined face (f), the position vector $\vec{r_f}$ is constructed from the centroid of the upwind (U) cell toward the downwind (D) cell intersecting the face centroid.

The simplest upwind-biased method available for calculating Φ_f is pure first-order upwinding (FOU). This scheme simply defines Φ_f to be equal to the value of Φ in the upwind cell, Φ_U in Figure 1. To obtain improved accuracy, the second-order upwinding (SOU) or linear reconstruction method is often employed. For this method, Φ_f is defined as:

$$\Phi_f = \Phi_U + \nabla\Phi \cdot \bar{r}_f \qquad (5)$$

where $\bar{r}_f$ is the position vector between the upwind cell centroid and the face centroid and $\nabla\Phi$ is the gradient of Φ in the upwind cell. The gradient must be computed numerically, for example, the Green-Gauss Theorem estimates the gradient as:

$$\nabla\Phi = \frac{1}{V} \sum_{f=1}^{\#\,faces} \tilde{\Phi}_f A_f \hat{n}_f \qquad (6)$$

in which V is the cell volume and $\tilde{\Phi}_f$ is an estimated value of Φ at the face centroid. For the simulations presented in this paper, the gradients for each cell are calculated by FLUENT using a cell-based method, in which $\tilde{\Phi}_f$ is set equal to the arithmetic average of the values of Φ at the neighbor cell centroids (e.g. Φ_U and Φ_D in Figure 1).

In most cases, a flux limiter is used in conjunction with the SOU scheme for calculating Φ_f. The default limiter in FLUENT tested in this study is that developed by Barth and Jespersen [7]. This method first determines limiting values Φ_{MIN} and Φ_{MAX} for each cell by finding the minimum and maximum Φ values from the set of all values at the centroids of its neighbor cells and the cell itself. Then the limiter value for each face is calculated by:

$$\begin{aligned} &\text{If } \Phi_f > \Phi_C \ : \ \alpha_f = MIN\{1, \frac{\Phi_{MAX} - \Phi_C}{\Phi_f - \Phi_C}\} \\ &\text{If } \Phi_f < \Phi_C \ : \ \alpha_f = MIN\{1, \frac{\Phi_{MIN} - \Phi_C}{\Phi_f - \Phi_C}\} \end{aligned} \qquad (7)$$

After each cell face is examined, the cell value of α is taken as the minimum of the face limiter values (constrained such that $\alpha \geq 0$), and Eq. (5) becomes:

$$\Phi_f = \Phi_U + \alpha \nabla\Phi \cdot \bar{r}_f \ . \qquad (8)$$

Conceptually, the Barth limiter enforces local monotonicity among the face values, in the sense that no reconstructed face value may result in a new extremum in the immediate neighborhood of the cell.

Non-local Non-monotonic (NLNM) Limiter

The current work details the development of a non-local, non-monotonic (NLNM) limiter. The introduction of non-locality into a limiter by the recursive examination of a cell's upwind neighbors reduces the chances of overly restricting the face values and "clipping" smooth regions of the variable field. At the same time, by ridding the solution of spurious local minima and maxima, oscillations are virtually eliminated. In

principle, the limiter operates similarly to the Barth limiter, but with a less restrictive bound on face and cell values, and without strictly enforcing local monotonicity. Face values may in fact introduce new extrema in the neighborhood of the cell, provided they are within the bounds determined for the cell from recursive reference to upstream cells.

As with the Barth limiter, the first step in the calculation of the NLNM limiter is to determine the appropriate maximum and minimum values that should be used to bound the dependent variable in the region of each cell. In contrast to the Barth limiter, this is done through recursive examination of upwind cell neighbor values, rather than examination of immediate upwind and downwind cell neighbors. The motivation behind the use of upwind neighbors only is that information is convected downstream, and in the absence of source terms any local extrema should depend only on upstream values of Φ.

We begin by defining the average inlet and outlet Φ values for a given cell:

$$\overline{\Phi}_{in} = \frac{\sum_{f:\dot{m}_f<0} \dot{m}_f \Phi_f}{\sum_{f:\dot{m}_f<0} \dot{m}_f} \tag{9}$$

$$\overline{\Phi}_{out} = \frac{\sum_{f:\dot{m}_f>0} \dot{m}_f \Phi_f}{\sum_{f:\dot{m}_f>0} \dot{m}_f}. \tag{10}$$

As expressed in Eq. (4), the face mass flow rate is,

$$\dot{m}_f = \rho_f \left(\hat{n}_j v_j\right) A_f \tag{11}$$

and positive values denote flow out of the cell. The convective change in the average value of the dependent variable across a given cell may be defined as:

$$\Delta\overline{\Phi} = \overline{\Phi}_{out} - \overline{\Phi}_{in}. \tag{12}$$

Note that, for the special case of steady state flow with no sources and no diffusion, the convective change is identically zero, according to the governing equation (Eq. 4).

Next, the maximum and minimum unlimited reconstruction values on downwind faces are determined for each cell. Since the reconstruction is linear, the extrema necessarily occur at nodes. Denoting these node extrema by Φ^*, they may be computed as follows:

$$\Phi^*_{MIN} = \min_{\substack{downwind \\ nodes}} \{\Phi_C + \nabla\Phi \cdot \bar{r}_n\} \tag{13}$$

$$\Phi^*_{MAX} = \max_{\substack{downwind \\ nodes}} \{\Phi_C + \nabla\Phi \cdot \bar{r}_n\} \tag{14}$$

where $\bar{r}_n$ is the relative position vector for each downwind node (Figure 2). The downwind nodes are defined as the set of nodes describing all faces of a cell for which the mass flow rate (Eq. 11) is positive. The reconstruction extrema defined by Eqs. (13,14) are used to enforce a "limit on the limit" based on the local variation of the dependent variable. For example, in regions with a uniform distribution of Φ, $\nabla\Phi = 0$ and $\Phi^*_{MIN} = \Phi^*_{MAX} = \Phi_C$.

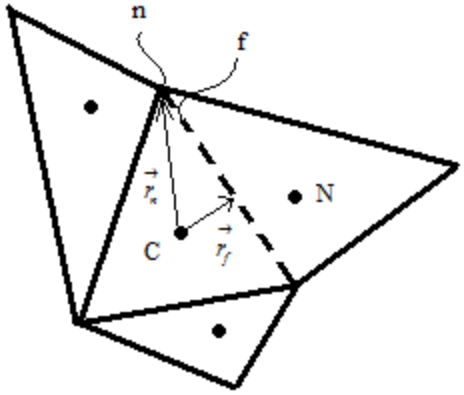

Figure 2. Unstructured Grid. For a given cell (C), the position vector $\vec{r_f}$ is drawn from the cell centroid to the face (f) centroid in the direction of the neighbor (N) cell. The position vector $\vec{r_n}$ is drawn from the cell centroid to the node (n), directed out of the cell.

The limiting values Φ_{MAX} and Φ_{MIN} for each cell are computed during each solution iteration through a recursive process that includes the following steps:

1. Initialize Φ_{MAX} and Φ_{MIN} in each cell to its centroid value Φ_C.
2. For each cell in the domain, loop through each of its upstream cell neighbors to determine the maximum and minimum upstream values as follows. First, limit each upstream neighbor value by the nodal extrema discussed above:

$$\Phi'_{MAX,nbr} = MIN\left(\Phi_{MAX,nbr}, \Phi^*_{MAX,nbr}\right) \tag{15}$$

$$\Phi'_{MIN,nbr} = MAX\left(\Phi_{MIN,nbr}, \Phi^*_{MIN,nbr}\right) \tag{16}$$

Next compute a maximum and minimum upstream value based on all upstream cell neighbor values:

$$\Phi''_{MAX} = MAX\left(\Phi'_{MAX,nbr}\right) \tag{17}$$

$$\Phi''_{MIN} = MIN\left(\Phi'_{MIN,nbr}\right) \quad (18)$$

3. Update the maximum and minimum values in each cell by taking into account the convective change as follows:

$$\Phi_{MAX,new} = MAX\left(\Phi''_{MAX} + \Delta\overline{\Phi}, \Phi_{MAX}\right) \quad (19)$$

$$\Phi_{MIN,new} = MIN\left(\Phi''_{MIN} + \Delta\overline{\Phi}, \Phi_{MIN}\right) \quad (20)$$

4. Repeat steps 2 and 3 for N iterations. Each iteration serves to include information from one additional level of upstream neighbors. For N→ ∞, the limiter in each cell is based on information from all of its upstream cell neighbors. In practice, it was found that N = 5 was sufficient to yield a close approximation to N→ ∞ without adding substantial computational effort to the simulation. All results in this paper were obtained with N = 5.

Once the maximum and minimum values for each cell have been thus determined, the fluxes are limited using the approach defined by Eqs. (7,8) above.

In order to implement this method into the FLUENT solver, the scalar variable Φ was defined as a User Defined Scalar (UDS), and the process of calculating the NLNM limiter was written as a User Defined Function (UDF). The output of the UDF was a source term defined for each cell by the summation of the difference between the limited projected face value, Φ_f, and Φ_C for each face. The discretization scheme for the solver was set to FOU; however, the algorithm was made second-order with the addition of the UDF source term.

DEMONSTRATION TEST CASES

To test the new limiter and its variations, several 2D, steady-state simulations were run. The domain was a unit square in the x- and y-directions. Two grids were used: one Cartesian with 100x100 cells and one unstructured triangular grid with 10,116 cells. The unstructured mesh intentionally used an edge length that yielded a cell count approximately equal to the Cartesian mesh. The simple test cases considered here are based on pure steady advection of a passive scalar Φ in a known incompressible velocity field, ***u***. Solutions are obtained with the second-order upwind scheme employing the new limiter (denoted SOU-N), and are compared to solutions from a first-order upwind scheme (denoted FOU), an unlimited second-order upwind scheme (denoted SOU), and a second-order scheme employing the Barth [7] limiter (denoted SOU-B).

For the first set of test cases, the limiters were tested for the case of a discontinuous variable field, to ensure that any non-physical oscillations were removed without introducing excessive amounts of dissipation. The bottom of the domain was set as an inlet with Φ = 0, while the left side of the domain was set as an inlet with Φ = 1. Two cases were run utilizing the structured grid. For the first, the velocity was uniform at an angle of 26.56° from the horizon; for the second, velocity was uniform at an angle of 45°. Figure 3 shows the contours of Φ for the SOU-B and SOU-N methods. It can be seen that the new limiter reduces the numerical dissipation of the discontinuity in the solution and maintains that reduction through the domain.

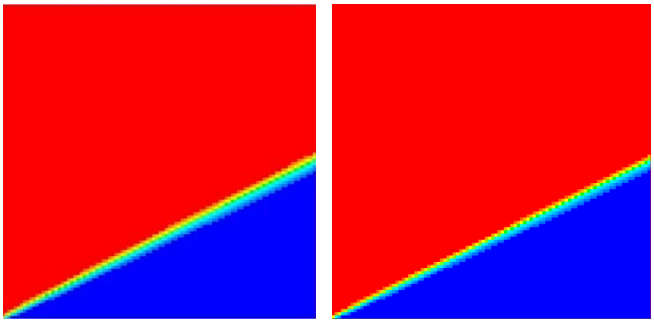

(a) **(b)**

Figure 3. Non-smoothed contours of Φ for the case of structured grid, uniform velocity angle of 26.56° and discontinuous variable distribution: (a) SOU-B ; (b) SOU-N.

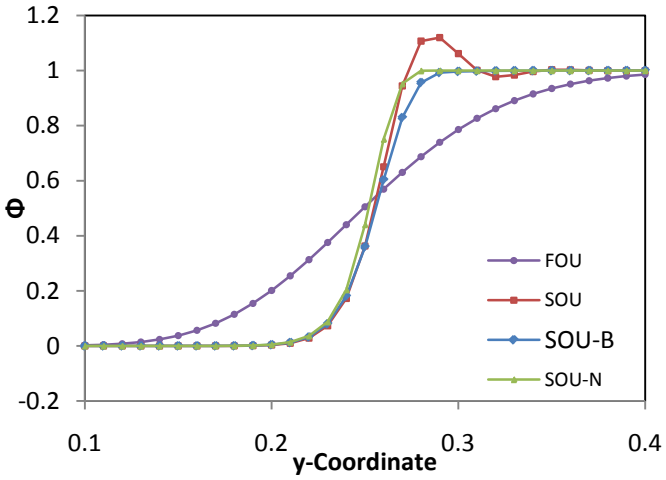

Figure 4. Plot of Φ vs y-Coordinate at x = 0.5 for FOU, SOU, SOU-B and SOU-N schemes for the 26.56° structured case.

Figure 4 compares the resolution of the discontinuity for the four methods tested. The plot shows the distribution of Φ in the y-direction at the location x = 0.5 in the domain. The difference in performance for each of the schemes used is apparent. The FOU scheme is, of course, excessively dissipative. The three second-order schemes exhibit key differences between themselves. The unlimited scheme (SOU) shows little dissipation, but also the expected variable overshoot, up to 12% higher than the maximum physical bound on the solution. The Barth limited (SOU-B) scheme

ameliorates the overshoot, but the limiter introduces some degree of smearing in the region of the interface. The new limiter (SOU-N) shows significantly less dissipation than the Barth limiter while eliminating the non-physical oscillations.

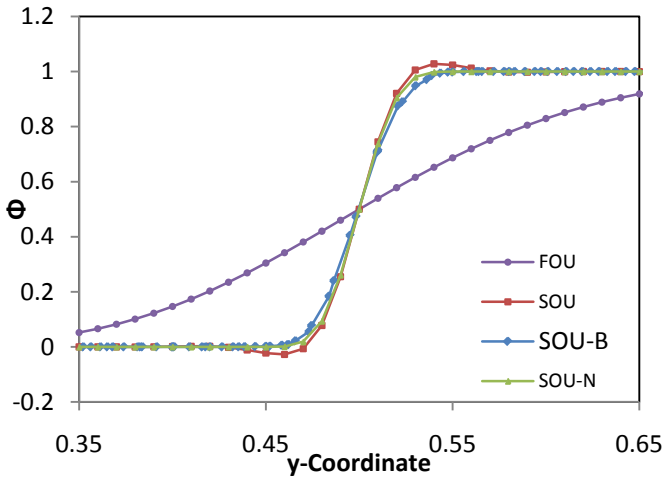

Figure 5. Plot of Φ vs y-Coordinate at x = 0.5 for FOU, SOU, SOU-B and SOU-N schemes for the 45° structured case.

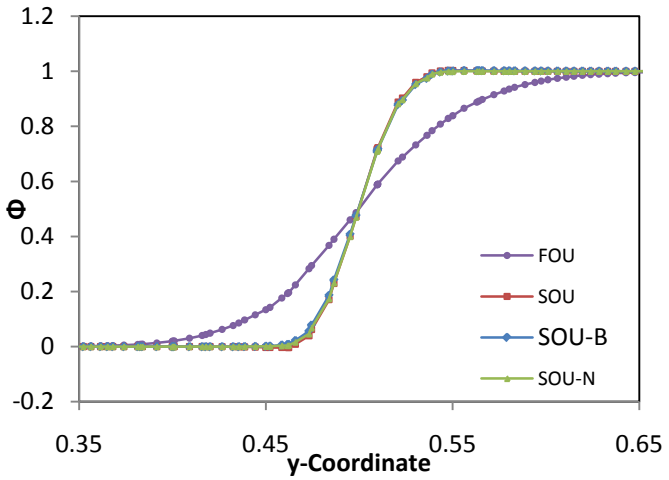

Figure 6. Plot of Φ vs y-Coordinate at x = 0.5 for FOU, SOU, SOU-B and SOU-N schemes for the 45° unstructured case.

Similar trends are seen on the structured grid with a velocity angle of 45°, as shown in Figure 5. For this case, the unlimited, second-order scheme shows variable over- and undershoot, which is eliminated by both limiting schemes. As above, the new limiter introduces less dissipation into the results. For the unstructured grid with a velocity angle of 45°, a similar plot is presented in Figure 6. In contrast to the structured grid results, only a small difference is noted in the dissipation levels of the two limited schemes. Also, the variable overshoot in the unlimited scheme is quite small (less than 0.3%). All three of the second-order methods, therefore, appear to be quite similar for resolving the discontinuity on an unstructured mesh.

To confirm that the naturally occurring extrema of a smooth function are maintained by the new limiting method, various sinusoidal inlet profiles of Φ were convected through the domain. Profiles with one, two, eight and twelve sine waves were applied to the left inlet boundary. As with the previous set of test cases, results were obtained for a structured grid with both uniform 26.56° and 45° velocity fields, as well as for an unstructured grid with a uniform 45° velocity field. For the single and double sine wave cases, the first-order method allowed some damping of the extrema; little difference was noted between the second-order methods, which all maintained the extrema throughout the domain. This result is expected since the smooth variations are very well resolved in these cases.

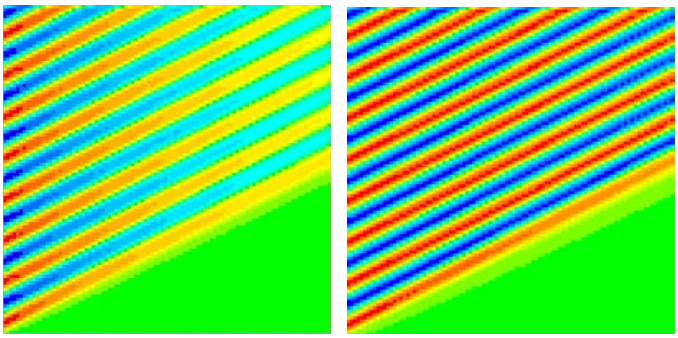

(a) **(b)**

Figure 7. Non-smoothed contours of Φ for the 26.56° structured eight sine wave case: (a) SOU-B; (b) SOU-N.

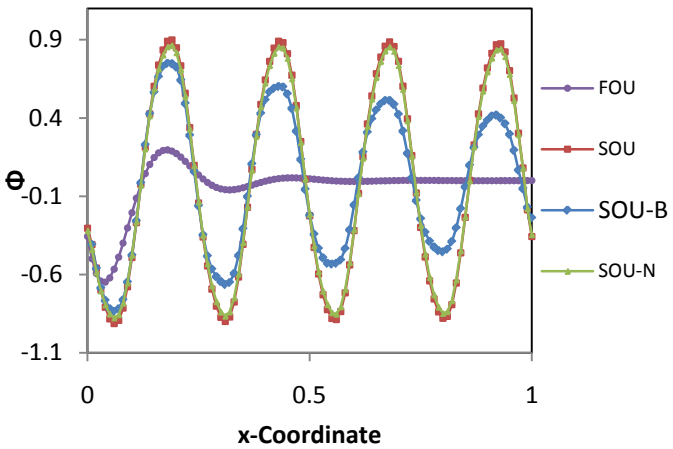

Figure 8. Plot of Φ vs x-Coordinate at y = 1.0 for FOU, SOU, SOU-B and SOU-N schemes for the 26.56° structured eight sine wave case.

As the number of sine waves at the inlet was increased, however, significant differences in the limiters became apparent. Data from the structured grid cases for an eight sine wave profile at the inlet are presented in Figures 7-9. From the contour plots in Figure 7, it can be seen that the new limiter is able to maintain distinct peaks and valleys in the convected sine waves throughout the entire domain, while the Barth limiter shows damping of the sine wave profile. This result is even

more apparent in Figures 8 and 9, which provide plots of Φ verses the x-Coordinate at the top (y = 1) outlet of the domain. For the 45° velocity case in Figure 9, the smallest peak for the SOU-B scheme is approximately 1/5 the height of the SOU-N limiter's peak at that same point.

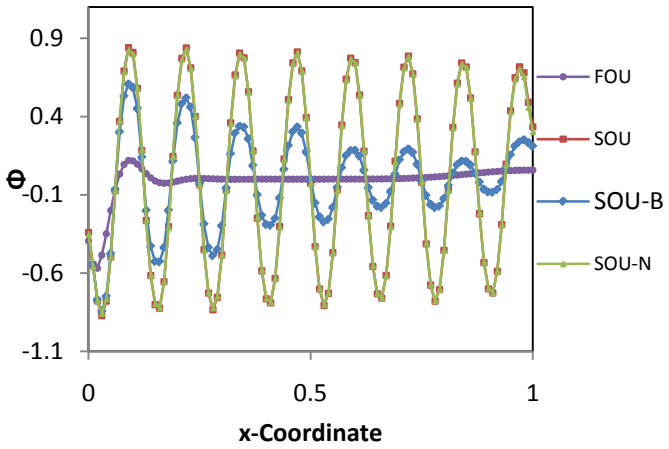

Figure 9. Plot of Φ vs x-Coordinate at y = 1.0 for FOU, SOU, SOU-B and SOU-N schemes for the 45° structured eight sine wave case.

As a measure of the performance of each scheme, the dissipation for each case was determined by:

$$D = -\int_{CS} \rho(\bar{v} \cdot \hat{n})\Phi^2 dA \qquad (21)$$

where $\hat{n}$ is the unit normal vector out of the domain, and the integration is performed over the entire domain boundary. The results of this calculation are presented for the specified cases in Table 1. For the 26.56° structured case, the new limiting scheme is 73.3% less dissipative than the Barth scheme; for the 45° structured case, the new limiter is 69.0% less dissipative.

The 45° unstructured case for eight sine waves is presented in Figures 10 and 11. As in the first set of test cases, the Barth limiting method performs better on the unstructured grid than on the structured grid, relative to the unlimited case. However, the new limiter still indicates an improvement over the Barth scheme; it is 37.1% less dissipative according to Table 1.

Table 1. Dissipation for Eight and Twelve Sine Waves.

Eight Sine Wave Cases				
	FOU	***SOU***	***SOU-B***	***SOU-N***
S26.56	0.812996	0.154687	0.664679	0.177257
S45	0.324133	0.118744	0.38235	0.118443
US45	0.507826	0.174735	0.316198	0.19869
Twelve Sine Wave Cases				
	FOU	***SOU***	***SOU-B***	***SOU-N***
S26.56	0.698829	0.542654	0.869068	0.530025
S45	0.426442	0.409287	0.412211	0.401727
US45	0.466747	0.412394	0.488172	0.411991

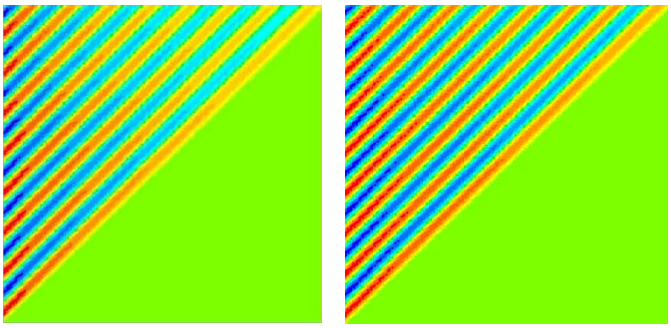

Figure 10. Non-smoothed contours of Φ for the 45° unstructured eight sine wave case: (a) SOU-B; (b) SOU-N.

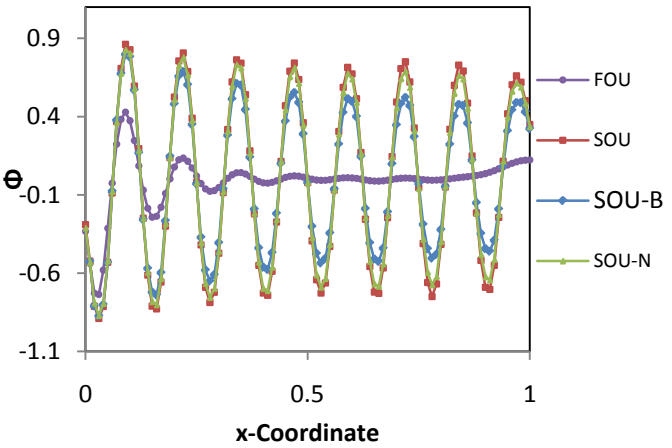

Figure 11. Plot of Φ vs x-Coordinate at y = 1.0 for FOU, SOU, SOU-B and SOU-N schemes for the 45° unstructured eight sine wave case.

The final convected sine wave simulations used a twelve wave profile at the inlet. The data from the structured 26.56° case is shown in Figure 12. For this case, the new limiter again shows very little dissipation of the natural extrema of the sine waves, compared to the unlimited second-order scheme. It is also noteworthy that the Barth limiting method performs only marginally better than the first-order method throughout half of the domain. The new limiter is 39.0% less dissipative than the Barth limiter for this case, according to the data presented in Table 1. Figure 13 presents similar results from the unstructured 45° case. Although the new limiting scheme is more dissipative in this case, it still shows an improvement over the Barth method and close agreement with the unlimited scheme. At the smallest peak in Figure 13, the solution employing the new limiter is approximately six times larger than that produced by the Barth limiter. For this case, the new limiter is 15.6% less dissipative than the Barth method. In each of these cases, the new limiter maintains the natural extrema of the sine waves almost as well as the unlimited second-order case.

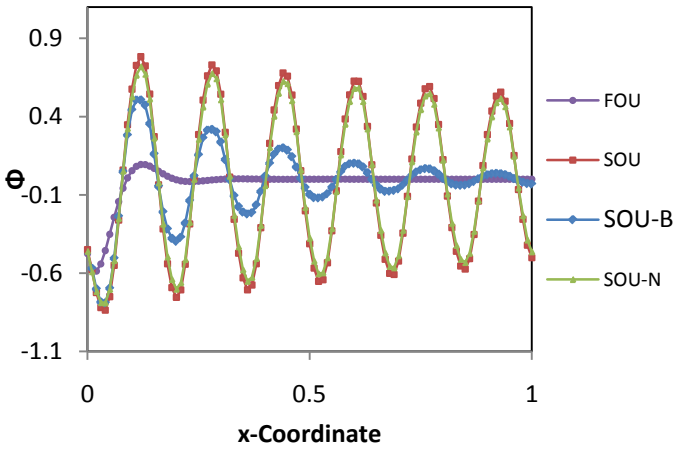

Figure 12. Plot of Φ vs x-Coordinate at y = 1.0 for FOU, SOU, SOU-B and SOU-N schemes for the 26.56° structured twelve sine wave case.

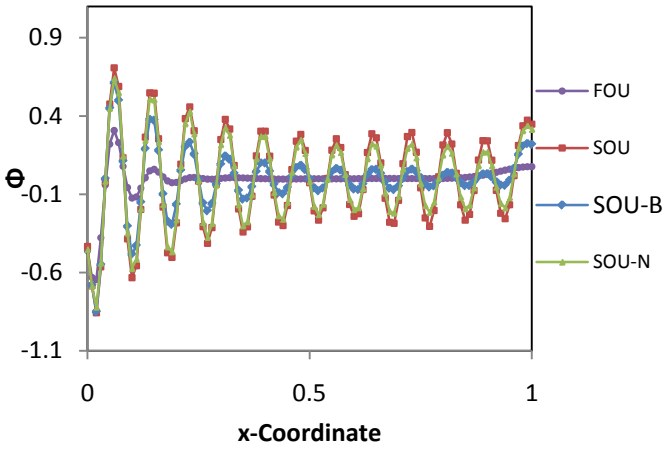

Figure 13. Plot of Φ vs x-Coordinate at y = 1.0 for FOU, SOU, SOU-B and SOU-N schemes for the 45° unstructured twelve sine wave case.

A final set of test cases was run to examine the limiter performance in a non-uniform velocity field. For these cases, the inlet of the domain was split into two regions, with the top region assigned a Φ value of 1, while the value for the bottom region was 0. The velocity through the domain was sinusoidal, with the discontinuity in Φ convected through the domain. Figure 14 shows contour plots for each of the second-order cases on the structured grid. The over- and undershoot in the unlimited (a) and the dissipation in the Barth limited (b) cases are apparent. Figure 15 plots the distribution of Φ vs. x through the domain at y = 0.5. From this plot, the non-physical extrema in the unlimited scheme are apparent, since the results exceed the physical bounds of 0 and 1. The Barth limiter causes a gradual decrease in the amplitude of the periodic distribution as the flow continues through the domain. As before, the new limiter produces results that are much less dissipative than those yielded by the Barth limiter, without the overshoot of the non-limited second-order method. Figure 16 shows the results on a similar plot as Figure 15 for each of the three schemes on an unstructured grid. As in previous cases, the first-order method is very dissipative. All the second-order methods perform much better, with the new limiting scheme being slightly less dissipative than the Barth limiting method. These results are consistent with all of those presented above.

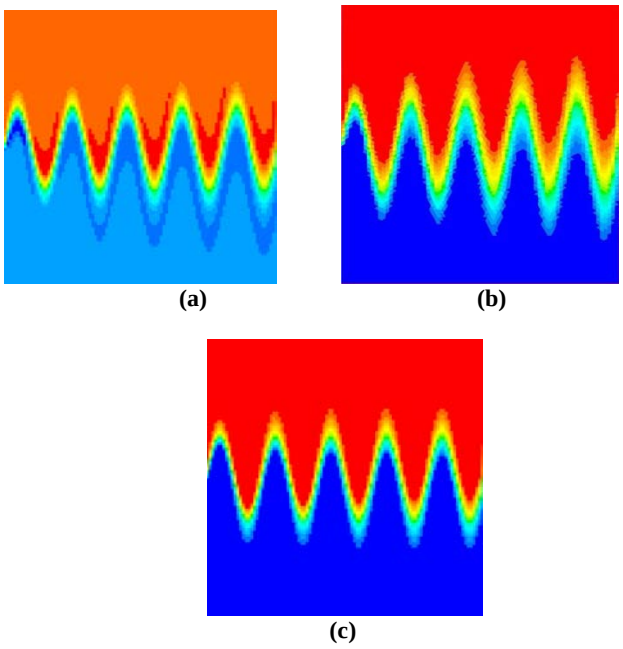

Figure 14. Non-smoothed contour plots of Φ for the structured non-uniform velocity case: a) SOU, b) SOU-B and c) SOU-N.

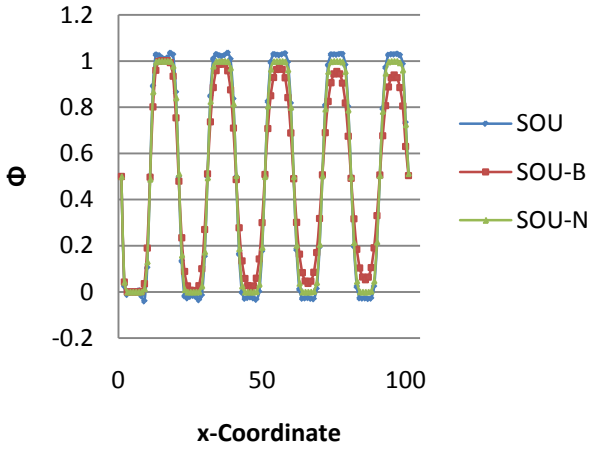

Figure 15. Plot of Φ vs x-Coordinate at y = 0.5 for SOU, SOU-B and SOU-N schemes for the structured non-uniform velocity case.

The computational cost and convergence rate for both limiting methods was also examined in this study. For the 26.56° velocity field structured grid cases, the methods exhibited nearly the same computational time per iteration. With the discontinuity inlet condition, the new limiting method maintained a slightly slower convergence rate than that of the Barth scheme. However, for the sine wave cases, the new

method converged at about the same rate as the Barth scheme. Results from the 45° velocity field structured grid were similar. The computational time and rate trends for the methods remained comparable, with one exception. Representative of the majority of the sine wave profile cases, Figure 17 demonstrates close agreement of the convergence rates. Figure 18 details the exception--the eight sine wave profile case. For this case, the Barth limiter case did not converge in to the same level as the new limiter case. For the 45° velocity field unstructured grid cases, the computational time per iteration trend was similar to the previous cases; however, both methods maintained the same convergence rate.

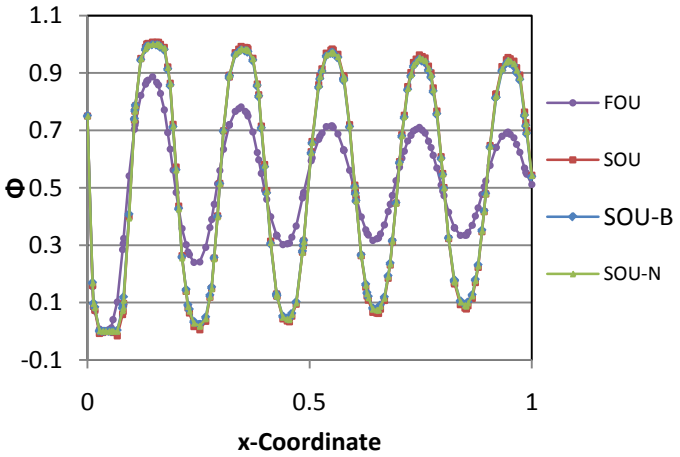

Figure 16. Plot of Φ vs x-Coordinate at y = 0.5 for FOU, SOU, SOU-B and SOU-N schemes for the unstructured non-uniform velocity case.

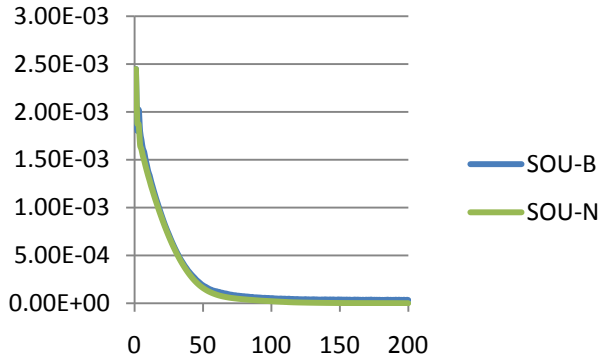

Figure 17. Plot of residual vs iteration for SOU-B and SOU-N, schemes for the 45° structured single sine wave case.

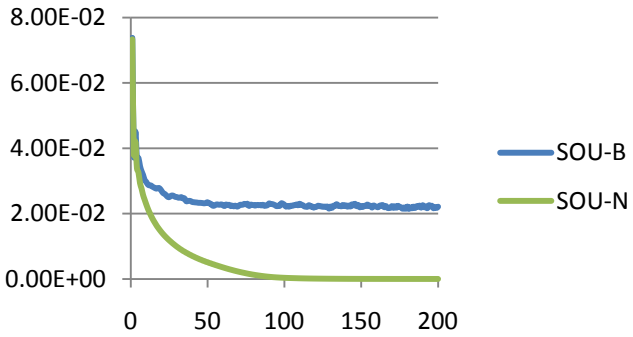

Figure 18. Plot of residual vs iteration for SOU-B and SOU-N on the 45° structrued eight sine wave case.

CONCLUSIONS

A new, non-local flux limiter was developed and applied to the solution of a scalar advection equation for various 2D, steady cases. The limiter utilizes recursive examination of upwind neighbor extrema to limit a given cell's minimum and maximum reconstructed face values. Solutions produced by the limiter were compared with those from first-order upwind and limited (employing the Barth limiter) and unlimited second-order upwind methods. The new limiter shows improvement over the existing methods in eliminating oscillations typically present in non-limited SOU schemes while reducing the numerical dissipation present in limited SOU schemes. Furthermore, for the majority of cases tested, the computational time and iterations necessary to reach convergence for the new method were approximately the same as those needed for the Barth limiter.

Future work includes applying the new limiter to the momentum equations and testing the scheme for complex, realistic flow conditions. Pending the success of these tests, a novel gradient calculation method will be developed for use in conjunction with the new limiter. It is anticipated that an optimum combination of limiter and numerical gradient calculation methods may lead to significant improvement in simulation accuracy for second-order discretization schemes.

ACKNOWLEDGEMENTS

This work was supported by the National Science Foundation through Grant No. CBET-0645138. The authors would like to thank Ansys, Inc. for their software support. The authors also appreciate the continued support of the administrative and technical personnel of the Mississippi State University High Performance Computing Collaboratory (HPC^2).

REFERENCES

[1] Godunov, S.K., 1959, "A Difference Scheme for Numerical Solution of Discontinuous Solution of Hydrodynamic Equations," Mathematicskii Sbornik, v. 47, pp. 271-306

[2] Hirsch, C., 2007, Numerical Computation of Internal and External Flows, Butterworth-Heinemann, Burlington, MA.
[3] Van Leer, B., 1974, “Towards the ultimate conservative difference scheme. II: Monotinicity and Conservation Combined in a Second Order Scheme,” Journal of Computational Physics, v. 14, pp. 361-370.
[4] Van Albada, G.D., et al., 1982, “A comparative study of computational methods in cosmic gas dynamics,” Astronomy and Astrophysics, v. 108, pp. 76-84.
[5] Roe, P.L. and Baines, M.J., 1981, “Algorithms for advection and shock problems,” Proceedings of the Fourth GAMM Conference on Numerical Methods in Fluid Mechanics, v. 5, pp. 281.
[6] Gaskell, P.H. and Lau, A.K.C., 1988, “Curvature-Compensated Convective Transport: SMART a New Boundedness-Preserving Transport Algorithm,” International Journal for Numerical Methods in Fluids, v. 8, pp. 617-641.
[7] Barth, T.J. and Jespersen, D.C., 1989, “The design and application of upwind schemes on unstructured meshes,” AIAA Paper No. AIAA-89-0366.
[8] Venkatakrishnan, V., 1993, “On the accuracy of limiters and convergence to steady-state solutions,” AIAA Paper No. AIAA-93-0880.
[9] Michalak, K. and Olliver-Gooch, C., 2008, “Limiters for Unstructured Higher-Order Accurate Solutions of the Euler Equations,” AIAA Forty-Sixth Aerospace Sciences Meeting.
[10] Yu, B., et al., 2001, “Discussion on Numerical Stability and Boundedness of Convective Discretized Scheme,” Numerical Heat Transfer: Part B, v. 40, pp. 343-365.
[11] Wei, Jin-Jia, et al., 2006, “A New General Convective Boundedness Criterion,” Numerical Heat Transfer: Part B, v. 49, pp. 585-598.
[12] Mengping, Z. and Ruxun, L., 1998, “Numerical Analysis and Construction of Limiter of High Resolution Difference Scheme,” Applied Mathematics and Mechanics, v. 19, no. 7, pp. 677-686.
[13] Tu, G. et al., 2006, “A Class of Compact Upwind TVD Difference Schemes,” Applied Mathematics and Mechanics, v. 27, no. 6, pp. 765-772.
[14] Tsui, Y. and Wu, T., 2009, “Use of Characteristic-based Flux Limiters in a Pressure-based Unstructured-Grid Algorithm Incorporating High-Resolution Schemes,” Numerical Heat Transfer: Part B, v. 55, pp. 14-34.
[15] FLUENT 6.2 User Manual, 2005, Fluent, Inc.